

Electronic Supporting Information (ESI)

**Nickel on Nitrogen-Doped Carbon Pellets for Continuous Flow
Catalytic Hydrogenation of Biomass-Derived Compounds in Water**

Francesco Brandi^a, Marius Bäuml^a, Valerio Molinari^a, Irina Shekova^a, Iver Lauer^a, Tobias Heil,^a Markus Antonietti^a and Majd Al-Naji^a

^aMax Planck Institute of Colloids and Interfaces, Am Mühlenberg 1, 14424 Potsdam, Germany

^bHelmholtz-Center Berlin for Materials and Energy, Schwarzschildstrasse 3, D-12489, Berlin, Germany

Materials

D-(+) Glucose Anhydrous (>99,5%), D-(-) Fructose (>99%), D-(+) Xylose (>99%), D-Sorbitol (>98%) and Vanillin (>99%) were supplied by Sigma Aldrich. Xylitol was provided by Laguma. Hydrochloric acid (0.1 M in water) was obtained from Merck. Vanillyl alcohol and 2-Methoxy-4-methylphenol (99%) were purchased from Acros Organics. Urea and Nickel Nitrate hexahydrate (>99%) were supplied from Roth. Zinc oxide nanoparticles (d = 20 nm) were ordered from Nanostructured and Amorphous inc. Semolina (type durum wheat) was purchased from the commercial brand Divella. The forming gas bottle (95/5) and H₂ bottle were purchased from Westfalia. Carbon black (CB) grains - Vulcan[®]-XC72R were furnished by Cabot.

Incipient wetness impregnation of 35 wt.-% Ni on NDC

A Ni catalyst supported on NDC pellet is consecutively prepared *via* incipient wetness impregnation. Before Ni impregnation, the washed and dried NDC pellets were kept under vacuum at 90° C for 12 h. To obtain the target metal loading, *i.e.*, 35 wt.-%, the appropriate amount (170 g) of Nickel nitrate hexahydrate (Ni(NO₃)₄ · 6H₂O) was dissolved in (110 cm³) of millipore water, followed by dropwise addition with continuous stirring of the aqueous Ni solution on the NDC dried pellets until complete saturation of the support pores. Subsequently, the impregnated pellets were dried again at 60° C in air for 12 h. Afterwards, the catalyst was calcined under N₂ atmosphere at 450°C. The temperature program of the calcination process consists of two steps: i) purging with N₂ at room temperature for 30 min; ii) increasing the temperature to 450° C with a heating rate of 3° C min⁻¹ and maintained for 2 h. Prior the catalytic experiments, the catalyst was reduced in forming gas (5 wt.-% H₂ and 95 wt.-% N₂) using the following program: i) 30 min of purging at room temperature, ii) increasing the temperature to 450° C with a heating rate of 3° C min⁻¹ and maintained for 5 h. For simplicity, the catalyst will be given a following code over all the manuscript: 35Ni/NDC. 35 refers to the Ni loading (35 wt.-%), NDC refers to the support (nitrogen-doped carbon). Similarly, the used catalysts will be annotated with (U_x) which refers to their use in Glu, Xyl and V hydrogenation.

Methodology for regeneration of Ni⁰ at spent catalyst

After the reaction, Ni⁰ at spent catalyst was regenerated through calcination procedure under air increasing the temperature to 300°C with a heating rate of 3°C min⁻¹ and maintained 3 h, followed by reduction step under forming gas (5 wt.-% H₂ and 95 wt.-% N₂) using the following program: i) 30 min of purging at room temperature, ii) increasing the temperature to 450° C with a heating rate of 3° C min⁻¹ and maintained for 5 h.

Products analysis and quantification

Reactants and products of the catalytic hydrogenation reactions were analysed using HPLC Agilent 1200 series equipped with a quaternary pump, diode array detector (DAD) and refractive index detector (RID). For the analysis of the products that derived from Glu and Xyl hydrogenation reaction, the HPLC system was equipped with Phenomenex Rezex ROA Organic Acid column (length 300 mm, 7.8 mm inner diameter) and RID was used as a detector. The analysis program was set to 45 min at 75° C using 0.1 wt.-% aqueous solution of formic acid as eluent with flow of 0.35 mL min⁻¹ and 3 µL as an injection volume. The retention time for the Glu, Sor, Fru, Xyl and Xyt was 18.0 min, 19.1 min, 19.9 min, 19.1 min and 21.4 min, respectively.

For V hydrogenation the HPLC was equipped with a C18 column (Hypersil GOLD C18 Selectivity LC Series) column and DAD was used as a detector. The DAD detector was used to ensure a complete

separation of the reactant and products due to the presence of characteristic chromophores. All measurements were conducted using a wavelength of 280 nm. The HPLC program included an injection volume of 3.0 μm at 35° C. The retention time was 15 min with an eluent flow of 1.2 mL min⁻¹. The eluent phase consists of an isocratic mixture of acetonitrile and water (50:50 vol.-%) has been used in the first 8 minutes.

Then, the column was washed with a non-isocratic solution of 100 % acetonitrile between the 8th and 12th minutes. Finally, the eluent composition has been reset to the initial isocratic phase at 15th minute. Prior the analysis, each sample was diluted with water (0.1 mL in 1 mL) to avoid saturation of the DAD with high concentrated solution (1 wt.-%). The retention time for the V, VA and MMP was 3.0 min, 2.7 min and 3.8 min, respectively.

The products were identified comparing the retention time with standards substances. The molar concentration (c_i) of the reactant and products was calculated from the integrated area of peaks and referred to calibration curve conducted with standard compounds.

The conversion and yield of the i -th compound (X_i , and Y_j) were calculated as reported in equation 2 and 3

$$X_i = \frac{c_i^0 - c_i^t}{c_i^0} \cdot 100\%$$

$$Y_j = \frac{c_j^t}{c_i^0} \cdot 100\%$$

where c_i^0 and c_i^t indicates respectively the initial reactant concentration and the reactant concentration at a distinct time.

Space time conversion (STCi) and space time yield (STY_j) normalized to Ni content were calculated as following:

$$\text{STC}_i (\text{mol}_i \text{h}^{-1} \text{mol}_{\text{Ni}}^{-1}) = \frac{c_i^0 - c_i^t}{n_{\text{Ni}} \cdot N_i^t}$$

$$\text{STY}_j (\text{mol}_j \text{h}^{-1} \text{mol}_{\text{Ni}}^{-1}) = \frac{c_j^t}{n_{\text{Ni}} \cdot N_i^t}$$

$$\tau (\text{h mol}_{\text{Ni}} \text{mol}_i^{-1}) = \frac{n_{\text{Ni}} \cdot N_i^t}{c_i^0}$$

Where n_{Ni} indicates the moles of Ni inside the reactor and N_i molar flow used (L h⁻¹).

Methods

Elemental analysis

Elemental analysis of C and N, was performed with a vario MICRO cube CHNOS Elemental Analyzer (Elementar Analysensysteme GmbH, Langensfeld) in the CHNS mode and the Ni and Zn content was determined by inductively coupled plasma optical emission spectroscopy (ICP-OES) using an Optima 8000 ICP-OES from PerkinElmer. Prior to the analysis, the samples (0.1 mg) were finely grinded and digested for 13 hours in 500 μL of Aqua regia solution (3:1 molar ratio of HCl and HNO₃, respectively).

X-ray diffraction (XRD)

Powder XRD measurement were performed on a Bruker D8 diffractometer equipped with a CuK_α source ($\lambda = 0.154 \text{ nm}$) and a NaI scintillation counter-Scinti-Detector. The diffraction pattern was recorded in the 2θ range between $4\text{-}70^\circ$ with steps of 0.05° and acquisition time of 2 sec per step. The Ni^0 crystallites size has been calculated applying the Scherrer equation at the reflection at $44^\circ \theta$.

$$B(\theta) = K\lambda / L \cos\theta$$

Where B is the size of the crystallites, L is the full width at half max (FWHM) calculated for the main reflection at the Bragg angle of $44^\circ\theta$. K is the shape factor of crystallites, herein, a spherical assumption has been made, with $K = 0.9$.

Thermogravimetric analysis (TGA)

TGA measurement has been performed using a Thermo Microbalance TG 209 F1 Libra (Netzsch, Selb, Germany). In a typical experiment, 0.01 g of sample were placed on a Pt crucible, dried at 150°C for 2 h and then heat to 1000°C with a heating rate of $10^\circ \text{C min}^{-1}$. The heating has been performed under a synthetic air flow of $20 \text{ cm}^3 \text{ min}^{-1}$. Previous to the analysis the samples has been dried for 6h at 363 K under vacuum,

N_2 sorption

N_2 sorption measurements were accomplished with N_2 at -196°C , after degassing the sample at 150°C for 20 hours under vacuum, using a Quantachrome Quadrasorb SI porosimeter. The specific surface area was calculated by applying the Brunauer-Emmet-Teller model in the relative pressure region of (0-0.05) for the adsorption branch (A_{BET}). The pore volume was calculated using the program QuadraWin. The pore size distribution and the average pore size were also determined using the program QuadraWin with the quenched solid functional theory (QSDFT) for slit/cylindral pores applied in the N_2 adsorption isotherm.

Scanning electron microscopy (SEM) and transmission electron microscopy (TEM)

The surface morphology and structure of the support and catalyst were investigated using SEM. The SEM images were taken using a Zeiss Lei Gemini 1550 microscope. Information about the dispersion of the Ni nanoparticles was obtained using transmission electron microscopy (TEM). The sample was prepared by dispersing (0.05 g) in ethanol in an ultrasonic bath for 10 min. Finally, the sample was placed onto a carbon-coated copper grid and dried at room temperature. The images were taken using an EM 912 microscopy (Omega/Carl-Zeiss Oberkochen) operating at 120 kV.

High-resolution scanning transmission electron microscopy (HR-STEM)

The HR-STEM images were acquired using a double-Cs-corrected JEOL ARM200F, equipped with a cold field emission gun and an energy-dispersive X-ray (EDX) filter. The acceleration voltage was set to 80 kV for the investigation.

X-ray photoelectron spectroscopy (XPS)

XPS measurements were conducted under ultrahigh vacuum (UHV) $1.5 \times 10^{-8} \text{ Pa}$ (CISSY equipment) equipped with a SPECS XR 50 X-ray gun with AlK_α (1486 eV) and Mg K_α (1254 eV) radiation source and

combined with a lens analyzer module (CLAM). The binding energy was calibrated with $\text{Au}4f_{7/2}$ as reference. The binding energy determination and the peak deconvolution has been made using “Igor” and “CasaXPS” software, for the background a Shirley function was used, while for the peak deconvolution a Voight function has been selected. Previous to the analysis the sample where grinded finely and dispersed on a top of a conducting tape and evacuate in UHV for 40 min.¹

Carbon monoxide temperature programmed desorption (CO-TPD)

CO-TPD measurements was performed using AMI-300 equipped with thermal conductivity detector (TCD) from Altamira Instrument. In each measurement, 0.05 g of catalyst was placed between two layer of quartz wool in the measurement cell (quartz U-tube). primarily, the sample was treated at 120°C in a flow He for 1 h. Afterwards, the sample was reduced by increasing the temperature to 450°C in the presence of a mixture of H_2 (20%) in He (80%) with a dwell of 4 h. Later, saturation of the catalyst with CO at 30°C was applied by flowing CO (20%) over the sample for 5 h. Then, the non-adsorbed CO was removed by flowing He (100%) over the sample for 30 min. To ensure a complete saturation of the samples, 20 pulses (509 μL each) of CO (20%) in He (80%) over the sample at 30°C. Finally, the CO desorption profile was recorded by increasing the temperature from 30°C to 550°C with 10°C min^{-1} with dwell of 30 min at 550°C.



Figure S1. The extrusion machine from La Monferrina P3.

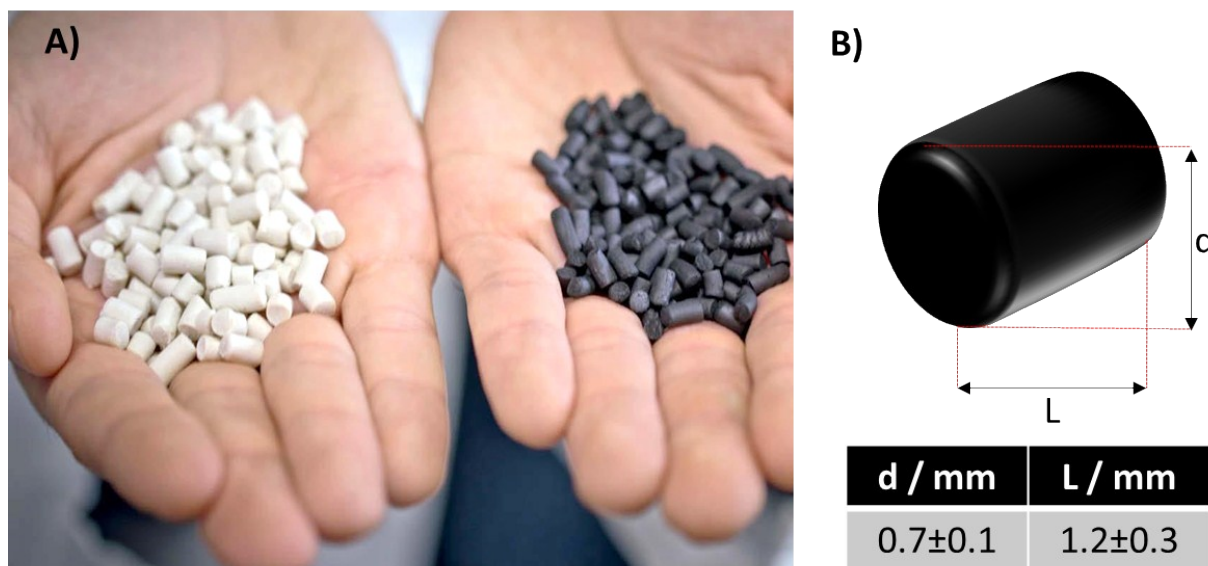


Figure S2. A) The raw carbon pellets after extrusion and the carbonized pellets,² B) Illustration representing a single pellet dimension, diameter (d) and length (L).



Figure S3. The reaction set up consists of A) HPLC pump equipped with pressure control B) heating unit (see the inner part of it at Figure S4) C) Mass flow controller for H₂ D) relief valve used for pressure controlling, connected with E) Sample collector.

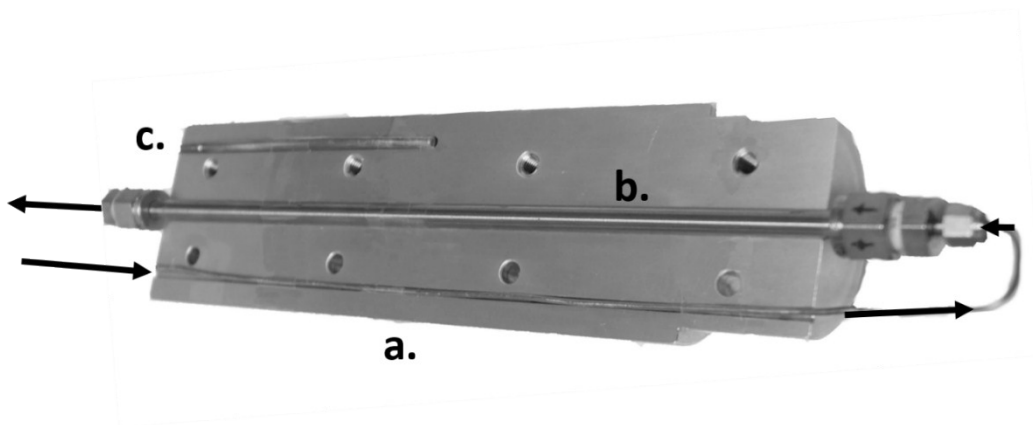


Figure S4. The homemade aluminum cylinder to be placed in the heating unit (from Figure S4), with three functional holes for the a) pre-heating unit, b) tubular reactor and c) thermocouple location.

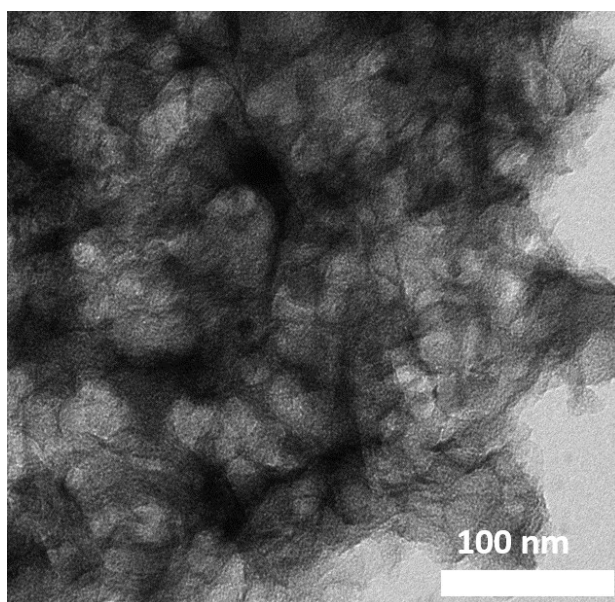


Figure S5. TEM pictures of NDC support. In the picture is visible the highly porous structure of NDC.

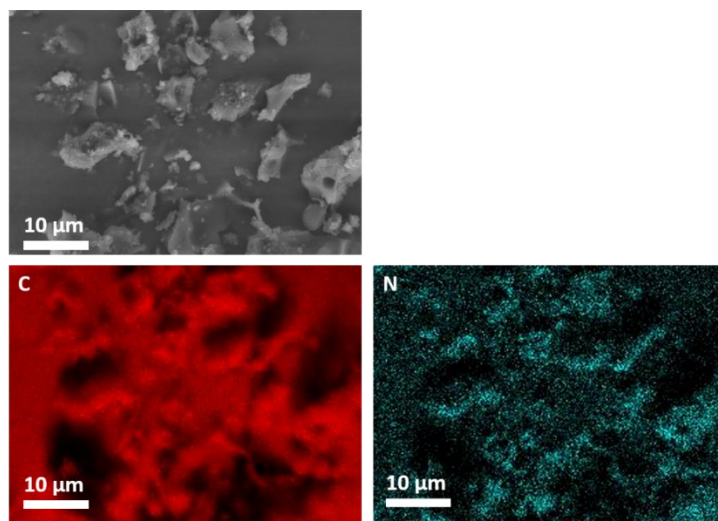


Figure S6. EDX mapping of the pristine NDC support. The upper left picture is the selected SEM area, while the EDX mapping is presented for C (red) and N (blue). The Black region in the C spectra represent a *shadowing effect* due to the thickness of the crashed pellets.

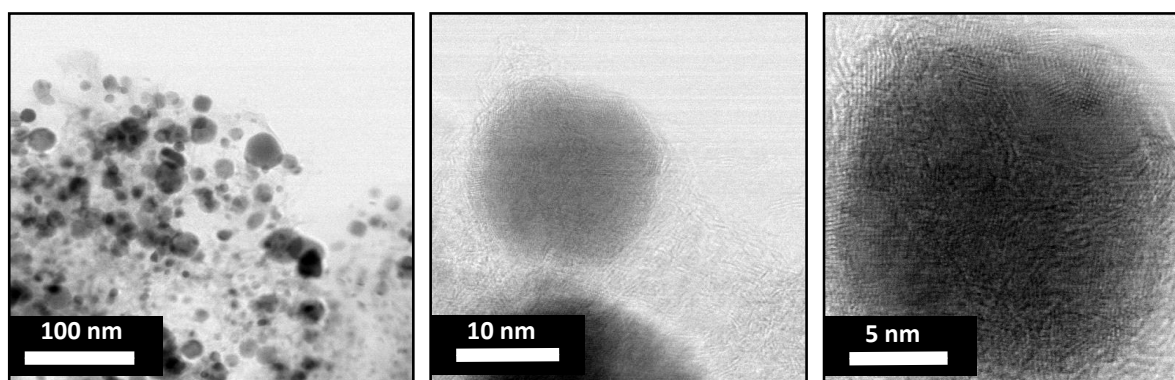


Figure S7. HR-STEM of the fresh 35Ni/NDC.

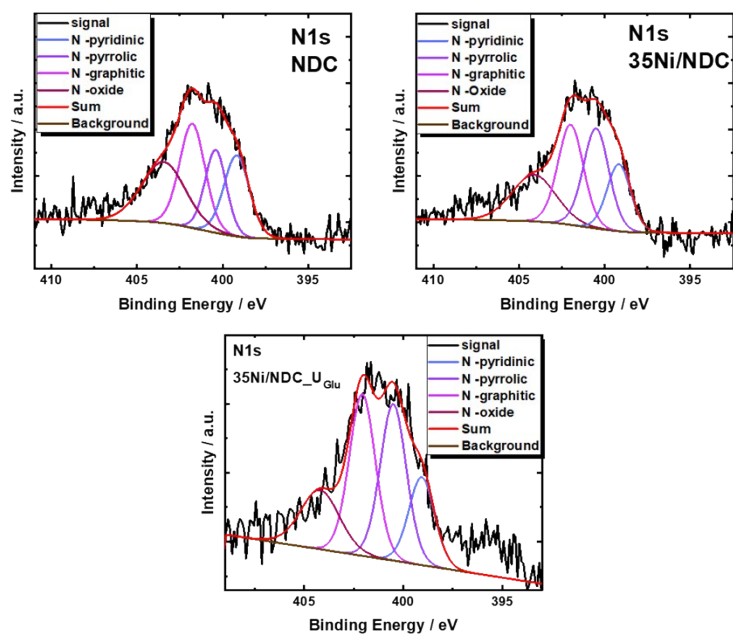


Figure S8. N1s XPS profile of the NDC support, the fresh 35Ni/NDC and the used 35Ni/NDC_U_{Glu} catalyst.

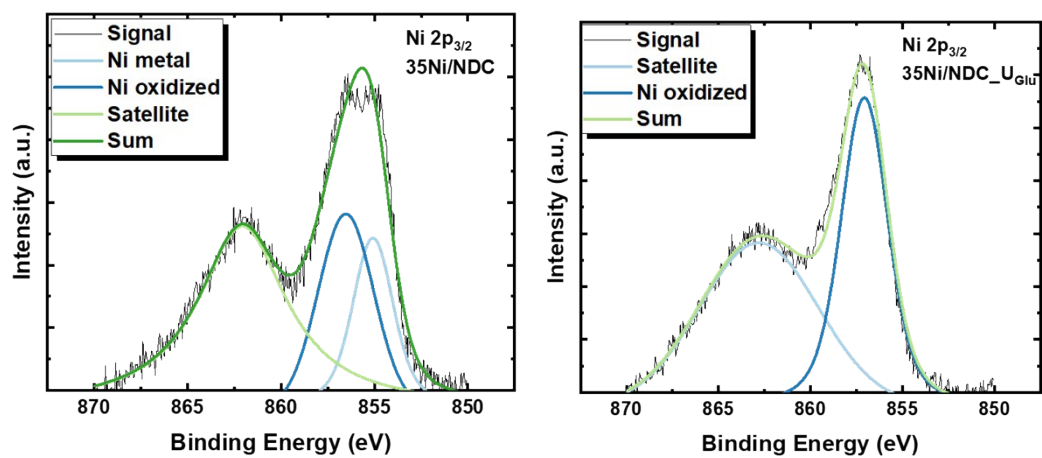


Figure S9. XPS spectra for the fresh 35Ni/NDC and spent catalyst in glucose hydrogenation (35Ni/NDC_U_{Glu}).

Table S1. Elemental composition of fresh 35Ni/NDC quantified via EDX that linked to HR-STEM.

Catalyst	C - K / At.-%	Ni-K / At.-%	O-K / At.-%
35Ni/NDC- nanoparticle region	20	67	11
35NiNDC- support region	94	3.8	1.7

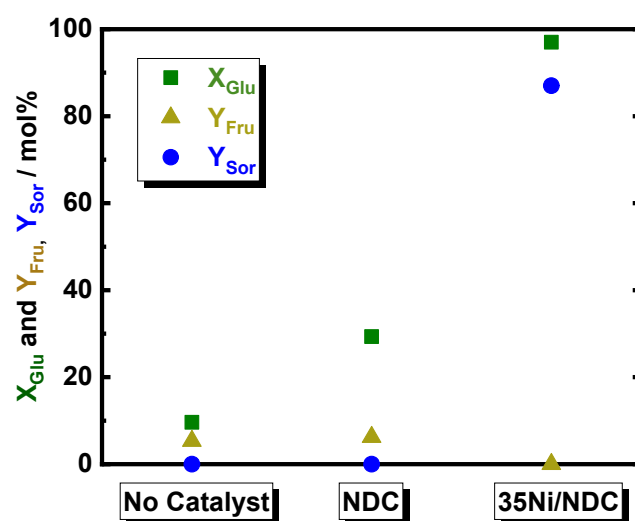


Figure S10. The conversion of glucose (X_{Glu}) and the yield of fructose and sorbitol (Y_{Fru} , and Y_{Sor}) in the absence of catalyst, in the presence of NDC and using 35Ni/NDC in the aqueous-phase hydrogenation of Glu to Sor; reaction conditions: $c_{\text{Glu}} = 56 \text{ mM}$ (1.0 wt.-%), $T = 150^\circ\text{C}$, $m_{\text{catalyst}} = 1.0 \text{ g}$, $Q_{\text{educt}} = 0.3 \text{ mL min}^{-1}$ ($\tau = 4.2 \text{ h mol}_{\text{Ni}} \text{ mol}_{\text{Glu}}^{-1}$), $Q_{\text{H}_2} = 15 \text{ mL min}^{-1}$, $p = 2.5 \text{ MPa}$.

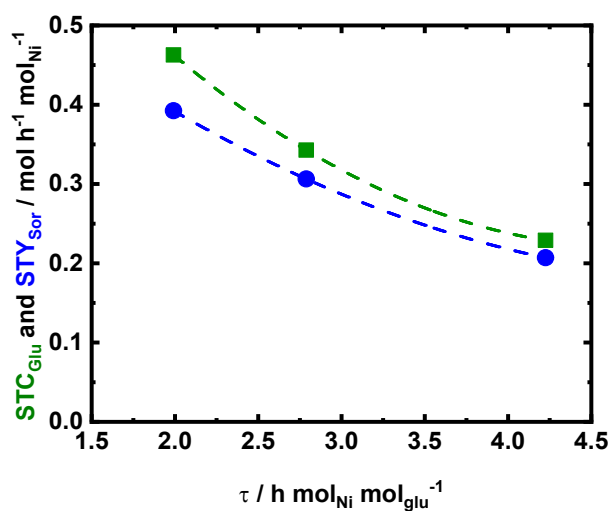


Figure S11. Space time conversion of Glu (STC_{Glu}) and space time yield of Sor (STY_{Sor}) as a function of space time " τ " using 35Ni/NDC in the aqueous-phase hydrogenation of Glu to Sor; reaction conditions: $c_{\text{Glu}} = 56 \text{ mM}$ (1.0 wt.-%), $T = 150^\circ\text{C}$, $Q_{\text{educt}} = 0.3, 0.5 \text{ and } 0.7 \text{ mL min}^{-1}$ ($\tau = 2.0, 2.8 \text{ and } 4.2 \text{ h mol}_{\text{Ni}} \text{ mol}_{\text{Glu}}^{-1}$), $Q_{\text{H}_2} = 15 \text{ mL min}^{-1}$ and $p = 2.5 \text{ MPa}$.

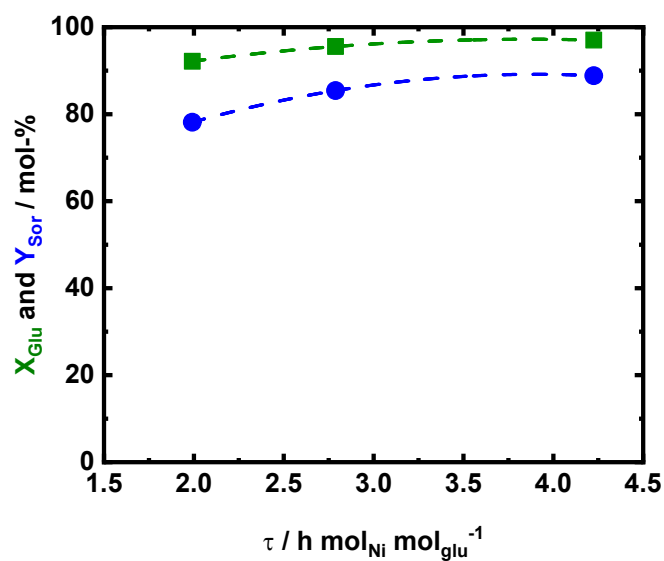


Figure S12. The conversion of Glu (X_{Glu}) and yield of Sor (Y_{Sor}) as a function of space time “ τ ” using 35Ni/NDC in the aqueous-phase hydrogenation of Glu to Sor; reaction conditions: $c_{\text{Glu}} = 56 \text{ mM}$ (1.0 wt.-%), $T = 150^\circ\text{C}$, $m_{\text{catalyst}} = 1.0 \text{ g}$, $Q_{\text{educt}} = 0.3, 0.5$ and 0.7 mL min^{-1} ($\tau = 2.0, 2.8$ and $4.2 \text{ h mol}_{\text{Ni}} \text{mol}_{\text{Glu}}^{-1}$), $Q_{\text{H}_2} = 15 \text{ mL min}^{-1}$ and $p = 2.5 \text{ MPa}$.

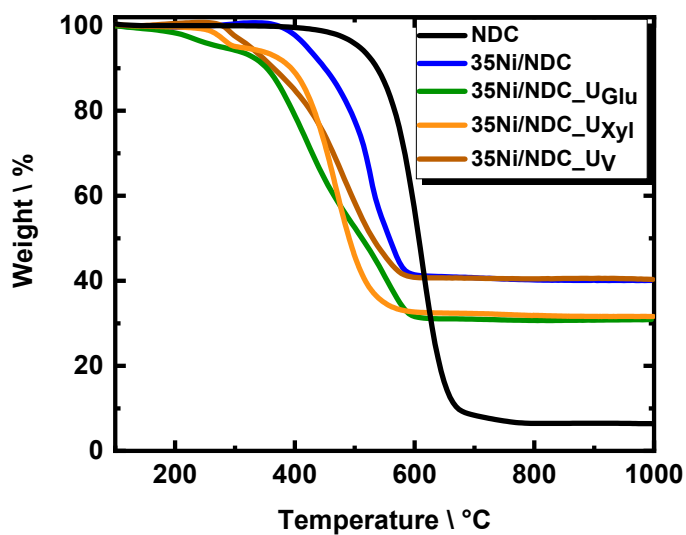


Figure S13. TGA in synthetic air, of the pristine NDC support, the fresh catalyst, 35Ni/NDC and the used ones, 35Ni/NDC_U_Glu, 35Ni/NDC_U_Xyl and 35Ni/NDC_U_V.

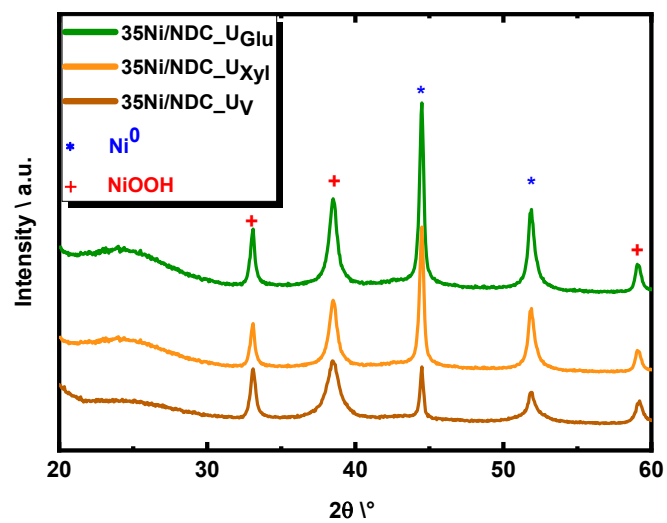


Figure S14. XRD diffraction patterns of spent catalysts 35Ni/NDC_U_{Glu}, 35Ni/NDC_U_{Xyl} and 35Ni/NDC_U_V.

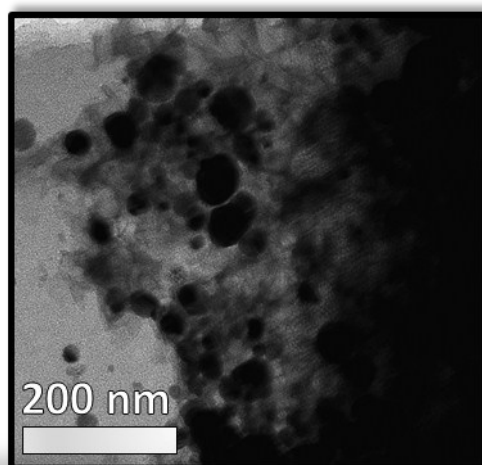


Figure S15. TEM image of spent catalyst (35Ni/NDC_U_{Glu}).

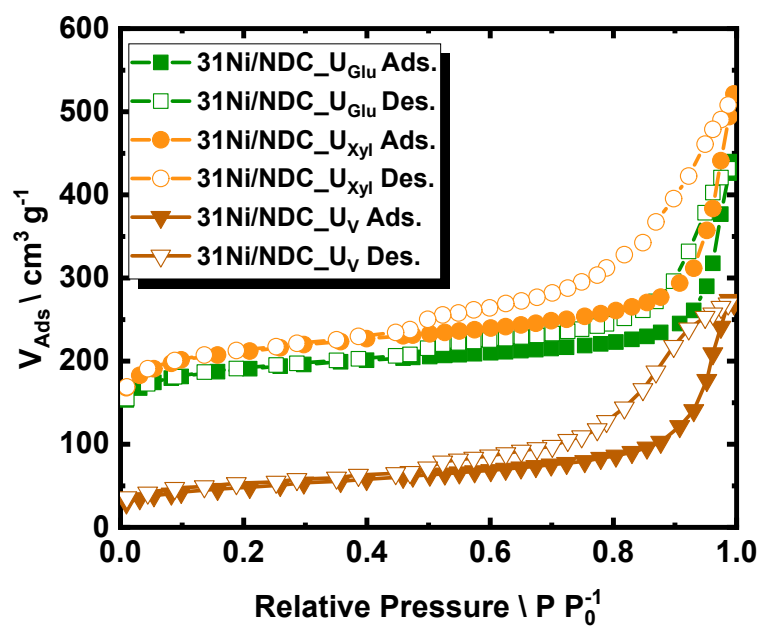


Figure S16. N₂ sorption isotherms of the spent catalysts measured at 77 K.

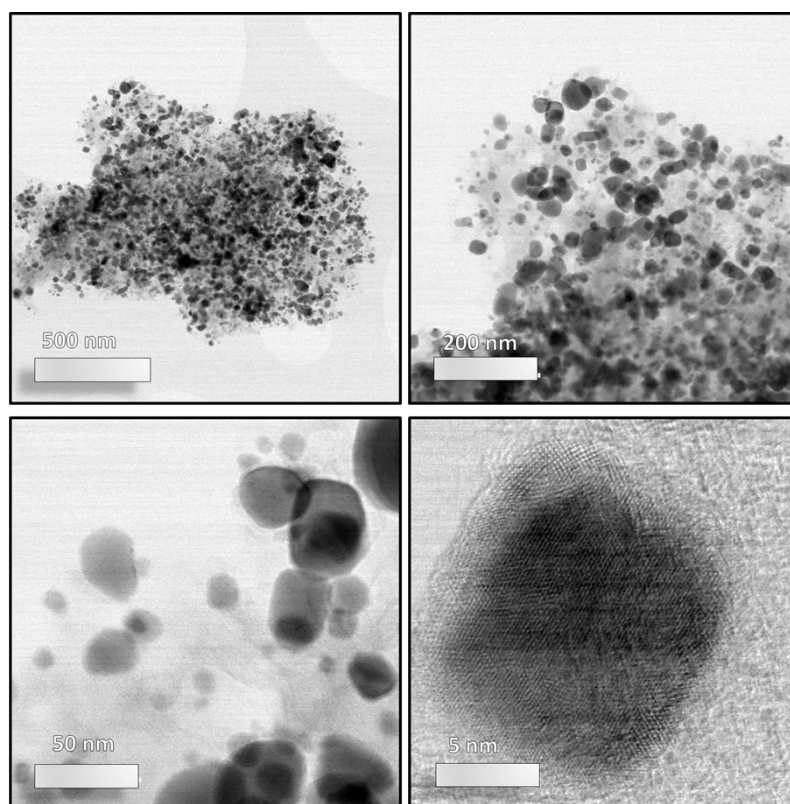


Figure S17 HR-STEM images of the regenerated 35Ni/NDC_R_{Glu}.

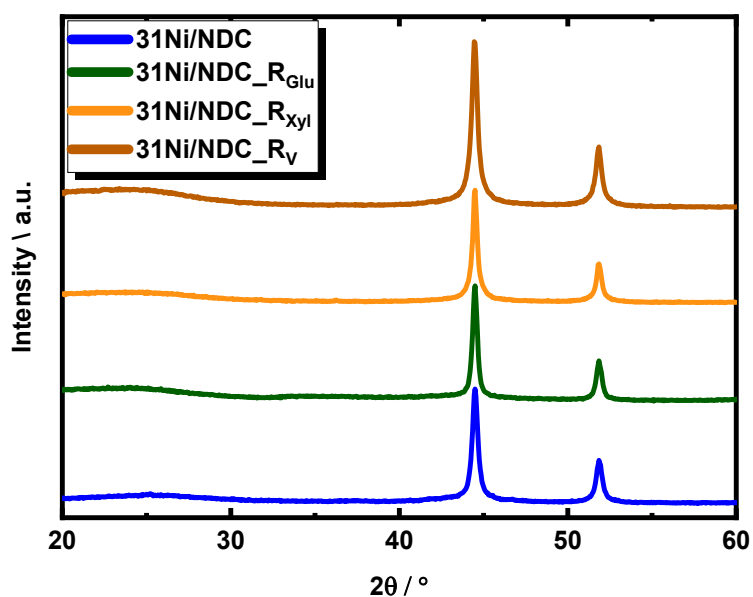


Figure S18. XRD diffraction patterns of regenerated catalysts 35Ni/NDC_R_{Glu}, 35Ni/NDC_R_{Xyl} and 35Ni/NDC_R_V, compared to the fresh one 35Ni/NDC.

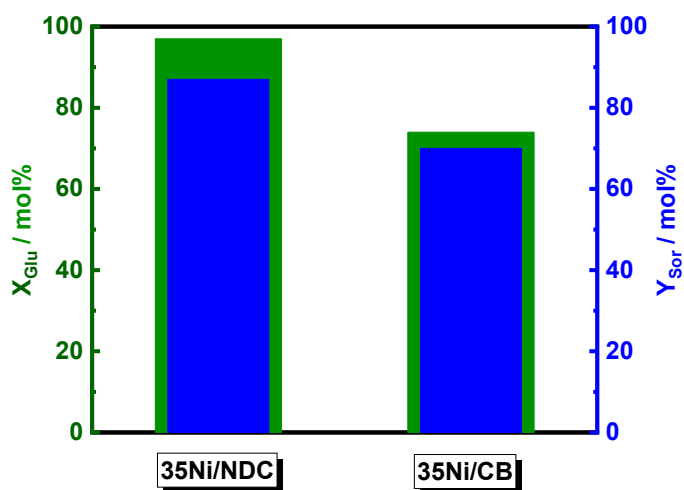


Figure S19. The conversion of glucose (X_{Glu}) and the yield of sorbitol (Y_{Sor}) over 35Ni/NDC and 35Ni/CB in the aqueous-phase hydrogenation of Glu to Sor; reaction conditions: $c_{\text{Glu}} = 56 \text{ mM}$ (1.0 wt.-%), $T = 150^\circ\text{C}$, $m_{\text{catalyst}} = 1.0 \text{ g}$, $Q_{\text{educt}} = 0.3 \text{ mL min}^{-1}$ ($\tau = 4.2 \text{ h mol}_{\text{Ni}} \text{ mol}_{\text{Glu}}^{-1}$), $Q_{\text{H}_2} = 15 \text{ mL min}^{-1}$, $p = 2.5 \text{ MPa}$.

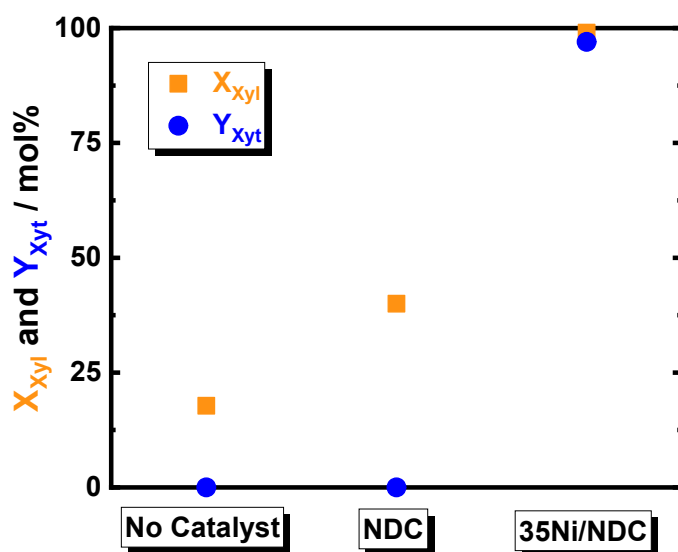


Figure S20. The conversion of Xyl (X_{Xyl}) and the yield of Xyt (Y_{Xyt}) in the absence of catalyst, in the presence of NDC and using 35Ni/NDC in the aqueous-phase hydrogenation of Xyl to Xyt; reaction conditions: $c_{Xyl} = 68 \text{ mM}$ (1.0 wt.-%), $T = 150^\circ\text{C}$, $Q_{educt} = 0.3 \text{ mL min}^{-1}$ ($\tau = 3.6 \text{ h mol}_{Ni} \text{ mol}_{Xyl}^{-1}$), $m_{catalyst} = 1.0 \text{ g}$, $Q_{H_2} = 15 \text{ mL min}^{-1}$, $p = 2.5 \text{ MPa}$.

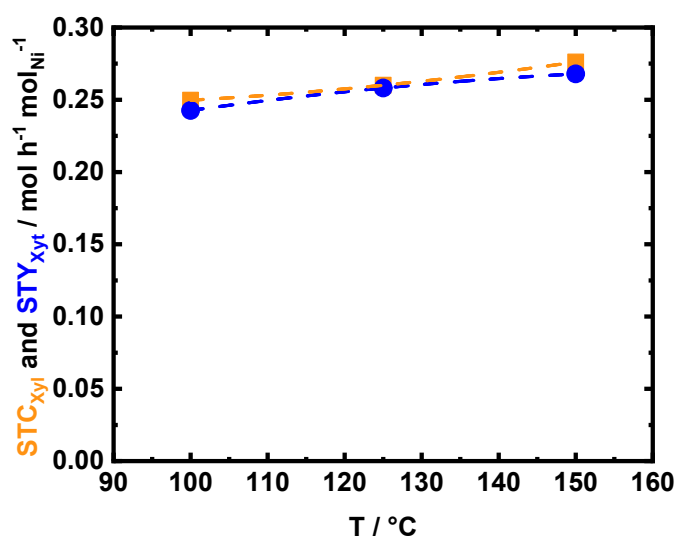


Figure S21. The space time conversion of Xyl (STC_{Xyl}) and space time yield of Xyt (STY_{Xyt}) as a function of temperature “T” using 35Ni/NDC in the aqueous-phase hydrogenation of Xyl to Xyt; reaction conditions: $c_{Xyl} = 68 \text{ mM}$ (1.0 wt.-%), $T = 100^\circ\text{C}$, 125°C and 150°C , $Q_{educt} = 0.3 \text{ mL min}^{-1}$ ($\tau = 3.6 \text{ h mol}_{Ni} \text{ mol}_{Xyl}^{-1}$), $Q_{H_2} = 15 \text{ mL min}^{-1}$, $p = 2.5 \text{ MPa}$.

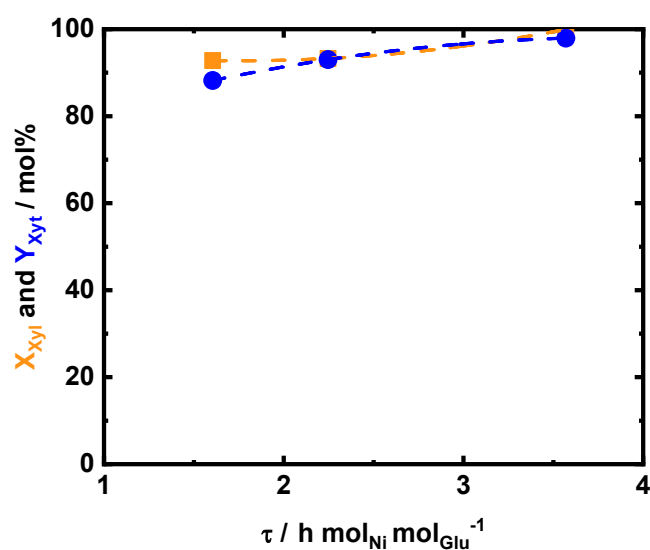


Figure S22. The space time conversion of Xyl (STC_{Xyl}) and space time yield of Xyt (STY_{Xyt}) as a function of the space time “ τ ” using 35Ni/NDC in the aqueous-phase hydrogenation of Xyl to Xyt; reaction conditions: $c_{\text{Xyl}} = 68 \text{ mM}$ (1.0 wt.-%), $T = 150^\circ\text{C}$, $Q_{\text{educt}} = 0.3, 0.5$ and 0.7 mL min^{-1} ($\tau = 3.6, 2.2$ and $1.6 \text{ h mol}_{\text{Ni}} \text{mol}_{\text{Xyl}}^{-1}$), $Q_{\text{H}_2} = 15 \text{ mL min}^{-1}$, $p = 2.5 \text{ MPa}$.

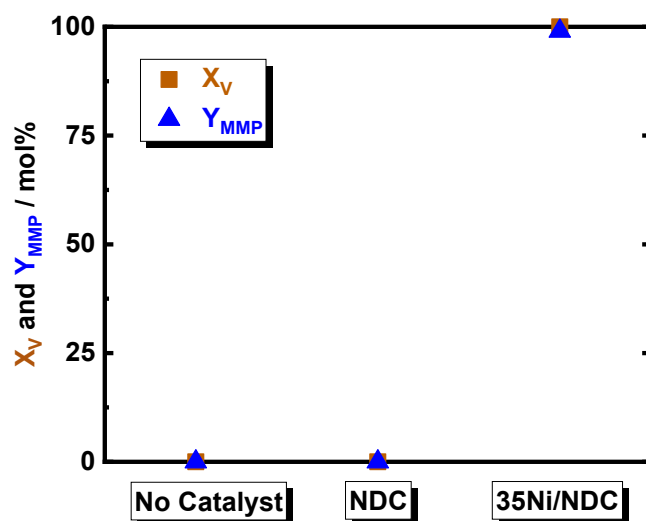


Figure S23. The conversion of V (X_{V}) and yield of MMP (Y_{MMP}) in the absence of catalyst, in the presence of NDC and using 35Ni/NDC in the aqueous-phase hydrogenation of V to MMP; reaction conditions: $c_{\text{V}} = 71 \text{ mM}$ (1.0 wt.-%), $T = 150^\circ\text{C}$, $m_{\text{catalyst}} = 1.0 \text{ g}$, $Q_{\text{educt}} = 0.5 \text{ mL min}^{-1}$ ($\tau = 3.4, \text{ h mol}_{\text{Ni}} \text{mol}_{\text{V}}^{-1}$), $Q_{\text{H}_2} = 15 \text{ mL min}^{-1}$, $p = 2.5 \text{ MPa}$.

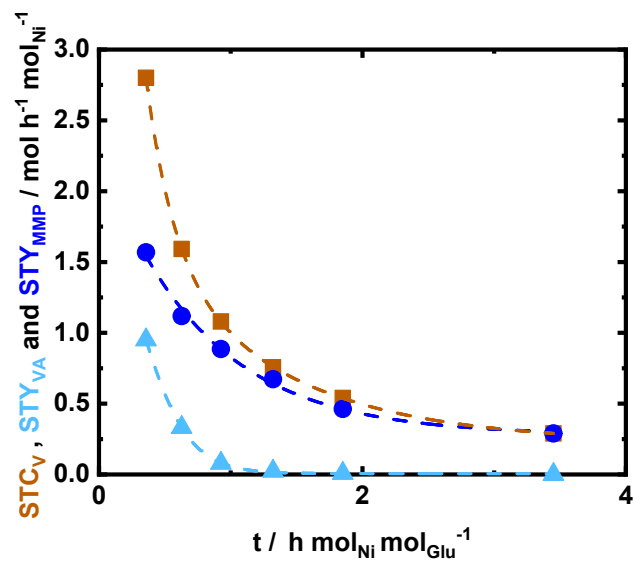


Figure S24. The space time conversion of V (STC_V), the space time yield of VA (STY_{VA}) and space time yield of MMP (STY_{MMP}) as a function of space time “ τ ” using 35Ni/NDC in the aqueous-phase hydrogenation of V to MMP; reaction conditions: $c_V = 72 \text{ mM}$, $T = 150^\circ\text{C}$, $Q_{\text{educt}} = 0.3, 0.5, 0.7, 1.0, 1.5$ and 3.0 mL min^{-1} (0.35, 0.63, 0.92, 1.3, 1.8, 3.5 $\text{h mol}_{\text{Ni}} \text{mol}_{\text{Glu}}^{-1}$), $Q_{\text{H}_2} = 15 \text{ mL min}^{-1}$ and $p = 2.5 \text{ MPa}$.

References

1. I. Lauermaann and A. Steigert, *Journal of large-scale research facilities JLSRF*, 2016, **2**, 67.
2. P. Hergtrtsberg and V. Molinari, *Max Planck Research Magazine*, 2019, **1-2019**, 66.